Available online at www.sciencedirect.com
ScienceDirect
Journal of Power Sources 161 (2006) 1324–1334
JOURNAL OF POWER SOURCES
www.elsevier.com/locate/jpowsour

Influence of the oxidative stabilisation treatment time on the electrochemical performance of anthracene oils cokes as electrode materials for lithium batteries

A. Concheso [a], R. Santamaría [a], R. Menéndez [a], R. Alcántara [b], P. Lavela [b,*], J.L. Tirado [b]

[a] *Instituto Nacional del Carbón, CSIC. Apartado 73, 33080 Oviedo, Spain*
[b] *Laboratorio de Química Inorgánica, Universidad de Córdoba, Campus de Rabanales,14071 Córdoba, Spain*

Received 28 November 2005; received in revised form 19 April 2006; accepted 30 April 2006
Available online 13 June 2006

Abstract

Three pitches derived from anthracene oils have been characterised in order to determine the effects of oxidative stabilisation by air blowing treatments of variable duration. From 6 to 12 h, significant changes are observed in both the morphological properties and the electrochemical behaviour as active materials in lithium test batteries. Continued oxidative treatment beyond 12 h led to high oxygen absorption resulting in less layered morphologies, highly irreversible capacities in the first cycle and low reversible capacities on subsequent cycling. Therefore, the beneficial effect of oxidative stabilisation requires a control of the annealing time to avoid an extended oxygen absorption and consequently a lower electrochemical efficiency of the carbon material when used as electrode in lithium batteries.

Keywords: Lithium battery; Anthracene oil; Oxidative stabilisation

1. Introduction

The use of graphite as anode material for Li-ion batteries has been extensively reported [1–4], being particularly attractive because of its low working potential versus lithium. Nevertheless, some deleterious effects must be overcome, such as the exfoliation arising from electrolyte intercalation [5] and relatively high costs of production. In addition, the continuous emergency of new cathode materials working at voltages near 5 V [6,7] favours a constant re-evaluation of anode materials with the aim of optimising the overall performance of the lithium battery. For instance, the high voltage cathodes allow an increase in the working potential of the anode, thus avoiding the electroplating effects that arise from maintaining intercalated graphite in a potential close to that of the Li^+/Li pair. In recent years, several families of compounds have been proposed as high-performance anodes, each based on different reversible lithium reactions. For example, lithium intermetallic compounds are formed from tin and antimony composites [8], classical insertion is involved in titanium spinel oxides [9], conversion reactions on transition metal oxides [10], while lithium storage in carbonaceous materials may include intercalation between graphene layers as well as interactions with other defect and surface sites [11].

Low temperature carbons are included in the latter group. Their use as negative electrodes for Li-ion batteries undoubtedly has economical advantages related to the reutilisation of side products derived from the petroleum industry. Moreover, the maximum theoretical capacity for an ideal graphite structure (LiC_6; 372 mAh/g) can be largely exceeded [12,13]. The highly disordered microstructure of low temperature carbons provides a great number of different sites where lithium can reversibly react with the carbonaceous materials, such as the interlayer space [14], or void spaces where heteroatoms such as oxygen and hydrogen are located and lithium can be reversibly linked [15].

In recent papers, we have demonstrated the improvement of the electrochemical performance in both isotropic and anisotropic phases submitted to oxidative stabilisation with air, prior to carbonisation [16,17]. This process favours the crosslinking between particles, which leads to a more stable car-

* Corresponding author. Tel.:+34 957 218 637; fax +34 957 218 621.
E-mail address: iq1lacap@uco.es (P. Lavela).

0378-7753/$ – see front matter © 2006 Elsevier B.V. All rights reserved.
doi:10.1016/j.jpowsour.2006.04.148

bon structure upon cycling. The thermal oxidative process preserves the carbon microstructure after pyrolysis, thus avoiding melting during further carbonisation up to the final temperature. The aim of this work is to evaluate the influence of oxidative stabilisation on the performance as electrode materials in lithium batteries of several cokes derived from anthracene oil.

2. Experimental

Three samples, named as AA2, AA3 and AA4, were obtained by air-blowing of anthracene oils at 450 °C and under a pressure of 5 bars and an air flow of 60 L h^{-1} for 6, 8 and 12 h respectively. The air-blown products were then distilled to adjust their softening point to either impregnating pitch (AA2, AA3) or binder pitch (AA4) specifications. These pitches were finally carbonised at 900 °C to obtain the anodic carbon materials, named as AA2(900), AA3(900), AA4(900).

Carbon, hydrogen, nitrogen and sulphur contents of pitches and cokes were determined using a LECO-CHNS-932 elemental analyzer. The oxygen content was measured using a LECO-VTF-900 graphite furnace. The softening point (SP) values were measured using a Mettler Toledo equipment according to the ASTM standard D3104-87. The carbon yield of the pitches was evaluated according to the Alcan method (ASTM D4715-87 standard) [18]. Pitches were analyzed by FTIR, using a Nicolet Magna IR-560 spectrometer equipped with mercury–cadmium telluride detector operating at 4 cm^{-1}. The diffusion reflectance spectra were converted to the Kubelka–Munk function. Aromaticity indices were calculated according to the method described in [19].

Optical microscopy analyses were carried out on using a polarised-light microscope Zeiss Axioplan equipped with a $1-\lambda$ retarder plate. For this purpose, each sample was previously polished. Scanning electron microscopy (SEM) was performed in a Jeol 200CX microscope. XRD patterns were recorded in a Siemens D-5000 equipment provided with a CuKα radiation. The interlayer distances were calculated from the 002 reflection. Crystallite size, Lc, was calculated from the Scherrer equation [20] with the Warren constants [21]. The refraction index used was 2.42 (graphite and other carbonaceous materials).

An Arbin potentiostat/galvanostat multichannel system was used to cycle two electrodes Swagelok type lithium cells at C/50 or C/10 rates for both charge and discharge branches. The working electrode consisted of a mixture of 92% active material and 8% PVDF binder coated on a copper foil of the same diameter. Counter electrode was a 9 mm discs of lithium metal. To assure the ionic conductivity between the electrodes a 1 M $LiPF_6$ (EC: DEC = 1:1) electrolyte solution was supported in Whatman glass fiber discs.

An Autolab PGSTAT12 system provided the electrochemical impedance spectra (EIS).

For this purpose, a three-electrode Swagelok type lithium cell, with a lithium metal reference electrode, was successively cycled, by passing current through the working and the counter electrodes, and allowed to relax in open circuit for at least 5 h before recording the impedance spectra at the end of the discharge. An AC voltage signal of 5 mV was applied from 100 kHz to 2 mHz.

Table 1
Chemical composition of the carbonaceous precursor pyrolysed at 450 °C

Precursor	AA2	AA3	AA4
C (%)	93.29	93.41	93.02
H (%)	3.75	3.72	3.58
N (%)	1.03	1.00	0.92
S (%)	0.59	0.56	0.57
O (%)	1.34	1.31	1.91
C/H	2.07	2.09	2.17
C/O	92.83	95.07	64.94
SP (°C)	96	98	134
TI (%)	21	25	39
NMPI (%)	2	7	16

SP: softening point; TI: insoluble phases in toluene; NMPI: insoluble phases in N-methyl-2-pyrrolidinone.

^{7}Li MAS NMR spectra were recorded in a Bruker Avance400WB instrument with a 4 mm diameter rotor and working at 14 kHz of spin rate. The ex situ measurements were carried out after extracting the electrodes from the discharged cell in a glove box. The electrodes were rinsed several times with solvent to remove the electrolyte. Then, the electrode was smoothly ground to powder and mixed with KBr to achieve a good homogeneisation of the sample into the hermetic holder. Reference was LiCl. The experimental spectra were deconvoluted using "dmfit program" [22]

3. Results and discussion

The chemical analysis of pitches treated at 450 °C (Table 1) show significantly higher oxygen content for AA4 sample. This fact undoubtedly influences some physical properties such as its high softening point or the most extended presence of phases insoluble in NMP and toluene [23]. These facts are directly related to carbon hardening because of the formation

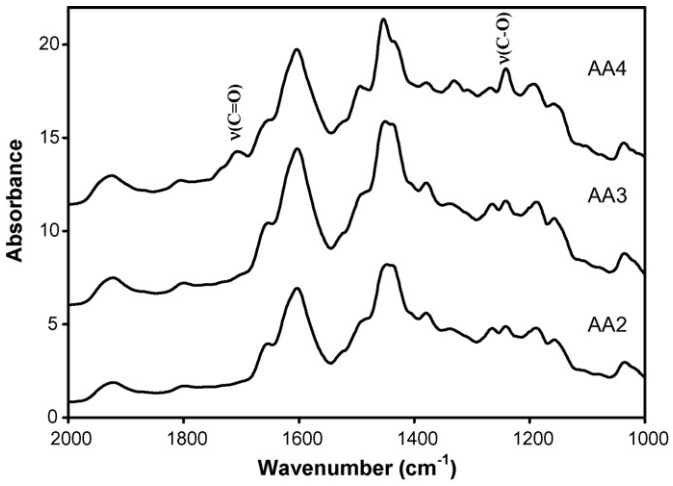

Fig. 1. FTIR spectra of pyrolysed samples obtained by air-blowing of anthracene oils at 450 °C for 6 (AA2), 8 (AA3) and 12 (AA4) hours. The labels on the spectrum of AA4 samples highlight the signals that reveal the presence of new oxygenated groups.

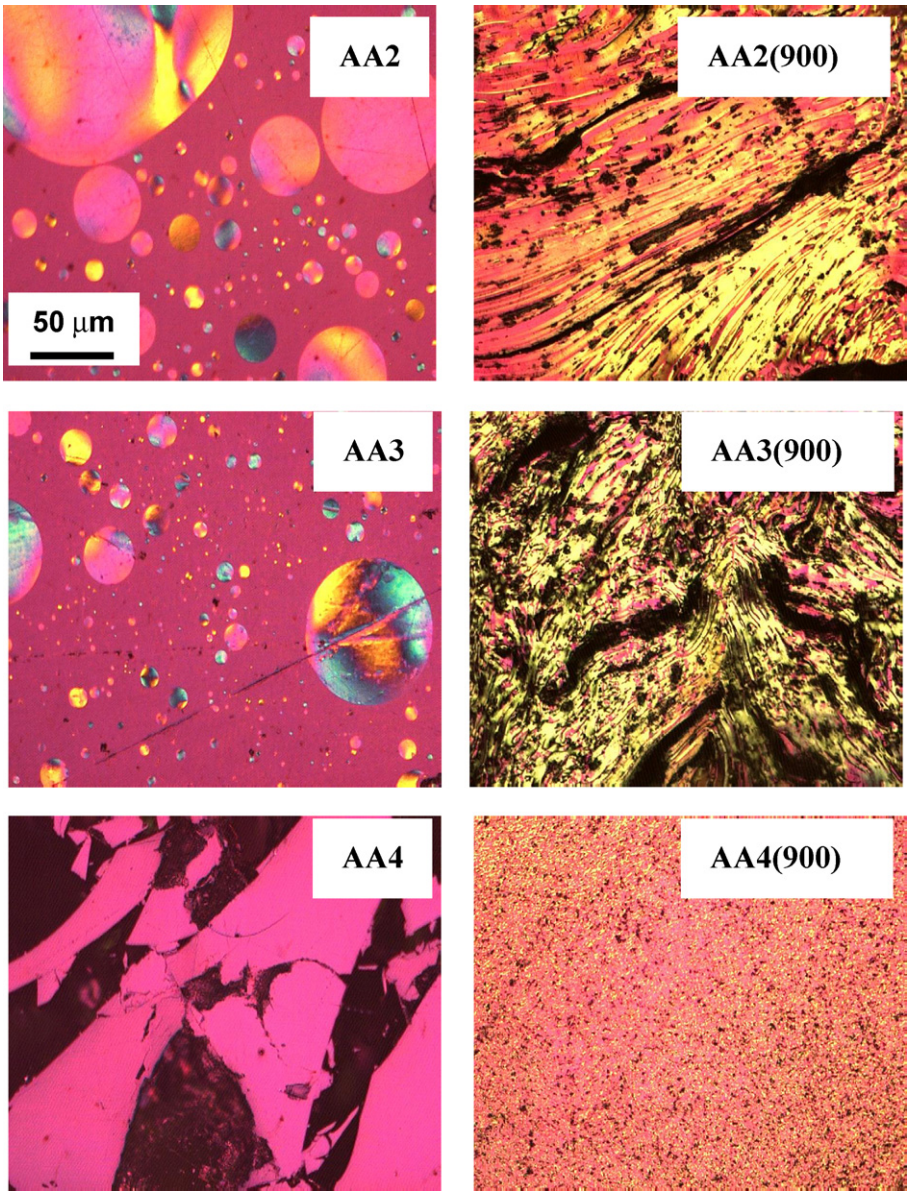

Fig. 2. Optical microscopy images of pyrolysed and carbonised samples.

of oxygen bridges between graphene particles. These links hinder the appropriated stacking of carbon layer occurring upon cabonisation, as will be further discussed from micrograph in Figs. 2 and 3. Fig. 1 displays the FTIR spectra corresponding to the precursors heated at 450 °C. Several features are common to all samples. Two intense signals at 1450 and 1600 cm^{-1} can be assigned to methyl substituents and C=C vibrations in the aromatics rings, respectively. The spectra corresponding to AA2 and AA3 pitches are qualitatively similar. However, as compared with the spectrum of sample AA4, two significant differences are visible. Firstly, the occurrence of a small band at 1698 cm^{-1} ascribable to C=O stretching vibrations in lactones or ester groups; and, secondly, a higher intensity peak at 1240 cm^{-1} due to C–O stretching vibrations evidence the higher content of oxygen in AA4 sample. These results are also reflected in the chemical composition of carbonised samples (Table 2). Thus, the oxygen content for AA4 was around five times higher than in the other samples (Table 2). The influence of heteroatoms such as oxygen on the electrochemical behaviour has been widely discussed. This element is attached to the carbon surface causing microstructural changes such as the elimination of defects

Table 2
Chemical composition of samples carbonised at 900 °C

Precursor	AA2 (900)	AA3 (900)	AA4 (900)
C (%)	97.51	97.37	95.29
H (%)	0.52	0.52	0.91
N (%)	1.40	1.49	1.64
S (%)	0.18	0.24	0.20
O (%)	0.39	0.38	1.96
C/H	15.63	15.60	8.73
C/O	333.37	341.65	64.82
d_{002} (Å)	3.512	3.523	3.578
Lc (Å)	16.79	16.01	13.78
La (Å)	38.37	42.24	47.22

or formation of oxide layers or microcavities. These modifications are usually considered responsible for net improvements in the electrode performance [23,24]. However, the presence of significant contents of oxygen and sulfur on the surface of pitches carbonised to 1000 °C leads to irreversibility in the first discharge, which is more marked as the content in heteroatoms increases [25].

The XRD patterns were characteristic of poorly ordered carbons with intense and broadened 002 and 110 reflections (not shown here). The interlayer distances calculated from the 002 reflection (Table 2) were significantly larger than that of graphite, as expected for non-graphitised carbons. Lc and La parameters were quite similar for all samples and no clear tendency could be discerned.

The optical textures of pitch and coke samples exhibit differences that deserve some comments (Fig. 2). AA2 and AA3 pitches have a characteristic texture of spherical mesophases with heterogeneous sizes, which is ascribed to the absence of quinolein insolubles. In contrast, AA4 exhibits large particles with cutting edges. These differences can be ascribed to the distinct chemical composition. Thus, the high oxygen content measured for AA4 pitch inhibits the presence of quinolein insolubles, which are responsible of the formation of the observed microbeads. The occurrence of these anisotropic phases upon carbonisation have been currently considered favourable for the electrochemical properties as a consequence of the low surface area and high packing density yielded by their spherical shape [26]. In fact, some chemical and physical treatments have been proposed to isolate these spheres from the isotropic phase [27,28].

The optical texture of carbonised samples was also quite similar for AA2(900) and AA3(900). Fluid domains were observed in both cases with more oriented particles for the AA2(900) sample, which are associated with the less viscous media in which the AA2 mesophase was formed. AA4(900) exhibited a very different picture characterised by a fine mosaic texture. Additional information about particle shape and surface roughness was obtained by the scanning electron microscopy observation of carbonised samples (Fig. 3). For AA2(900) and AA3(900), the micrographs show particles with heterogeneous sizes and the occurrence of regularly stacked layered material. The SEM micrographs for the AA4(900) sample show larger particles with flatter surfaces in which the stacking of carbon layers has not been yet developed probably due to the extended air blowing process. In fact, it is well documented that oxygen acts as a crosslinker, which reduces, or even inhibits, the mobility of basic structural units that favours the layer stacking. Henceforth, a longer treatment and hence a higher oxygen content in the sample contributes to bridge the graphene particles, thus hindering the condensation of graphene layers upon carbonisation [29].

Fig. 4 shows the first five galvanostatic cycles of the lithium cells built up with the carbonised samples as working electrodes. The galvanostatic charge–discharge curves exhibit a sloping voltage variation usual in these low temperatures carbons. The general profile differs from that of graphitic materials. In low temperature carbons, the microstructural disorder creates sites with a range of chemical environments developing a wide range

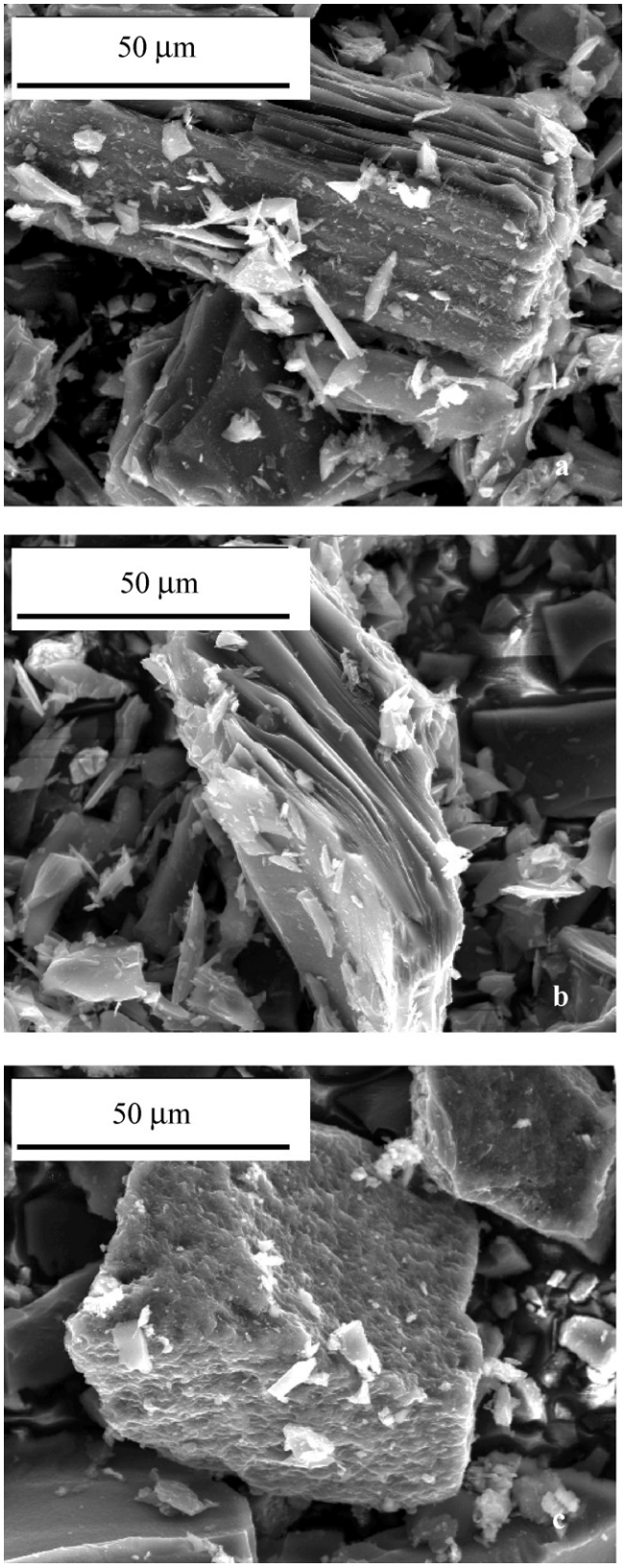

Fig. 3. SEM micrographs of carbonised samples (a) AA2(900), (b) AA3(900) and (c) AA4(900).

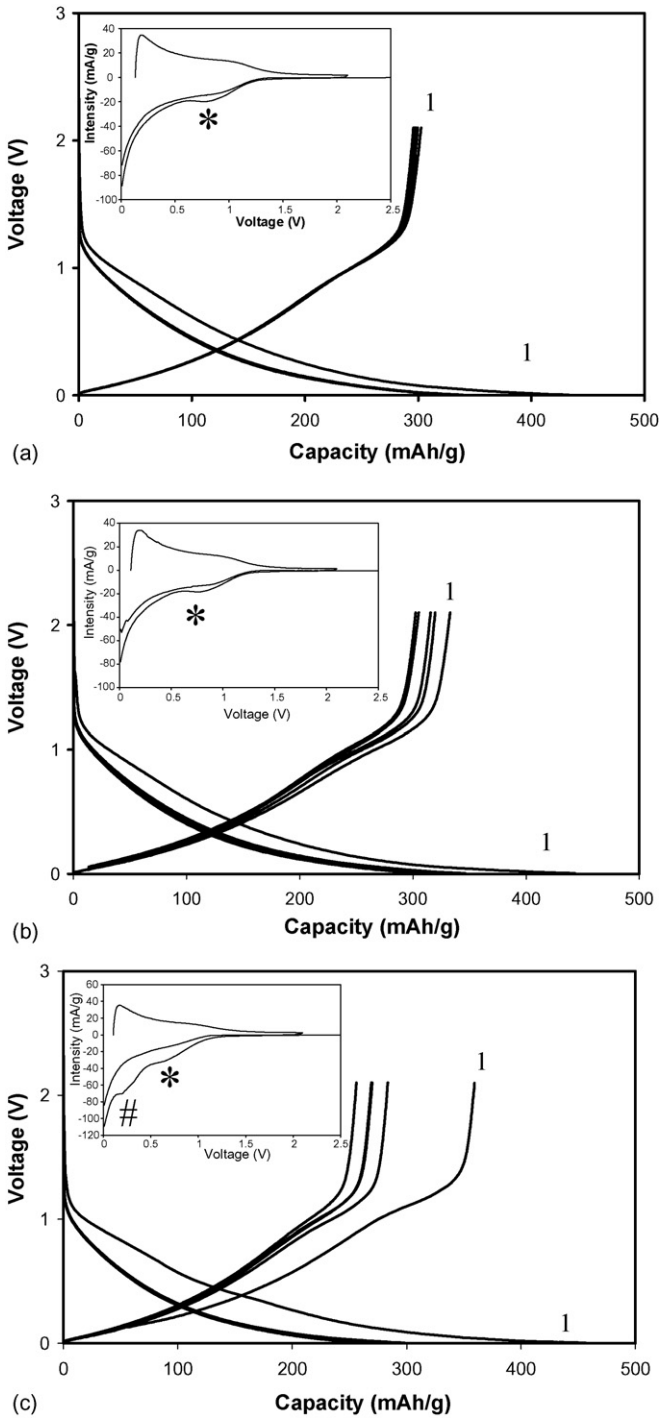

Fig. 4. Galvanostatic charge and discharge branches (first five cycles) of the carbonised samples (a) AA2(900), (b) AA3(900) and (c) AA4(900) using a C/50 kinetic rate. First charge and discharge curves have been marked.

of potential, which is reflected in a sloping potential in the capacity curves. The first discharge has a different profile as compared with further discharges. This fact is ascribed to irreversible reactions of lithium with surface-active groups or electrolyte decomposition processes that give by-product layers on the carbon surface. The resulting film has a passivating effect that hinders the extended loss of capacity in successive cycles. The overall process is evidenced by the occurrence of a quasi-plateau between 0.8 and 1.2 V. This electrochemical process can be better resolved by the potentiostatic method. The insets in Fig. 4 correspond to the I versus V plots of the first two discharges and first charge. The barely discernible quasi–plateaus in the V versus capacity plots obtained by the galvanostatic method are now revealed as bands. The asterisks highlight the position of the band ascribable to SEI formation. The area of this band is qualitatively higher for AA4(900) indicating a more extended irreversible reaction of formation of the passivating layer for this sample. The lack of reversibility of the SEI formation is evidenced by the low reproducibility of this quasi-plateau in subsequent cycles. Moreover, AA4(900) shows another quasi-plateau at ca. 0.3 V (marked as # in Fig. 4), which is absent in the others samples. Dahn et al. have detected a similar feature in pregraphitic carbons with higher oxygen and sulphur contents [25]. Li is irreversibly trapped by these hetero-elements. This fact agrees with the higher oxygen content of AA4(900) sample as compared with the others (Table 2). All these irreversible reactions are responsible of the differences in working potential between the first and subsequent discharges.

Henceforth, the high contribution of irreversible processes during the first discharge for AA4(900) leads to high capacity values. The absence of these electrochemical reactions in second and successive discharges, where capacity arises mainly from

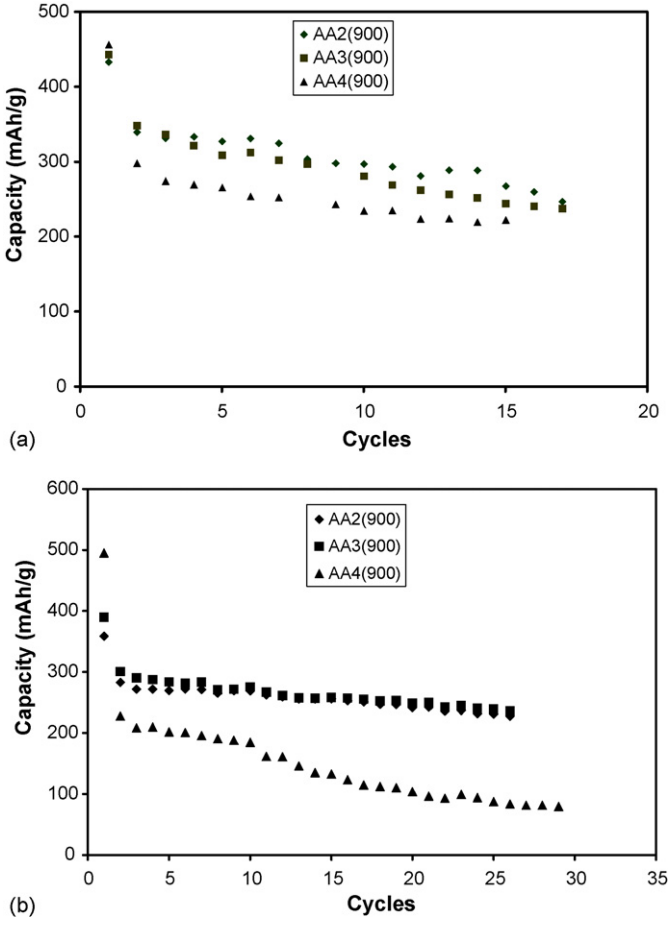

Fig. 5. Extended galvanostatic cycling of the carbonised samples at (a) C/50 and (b) C/10.

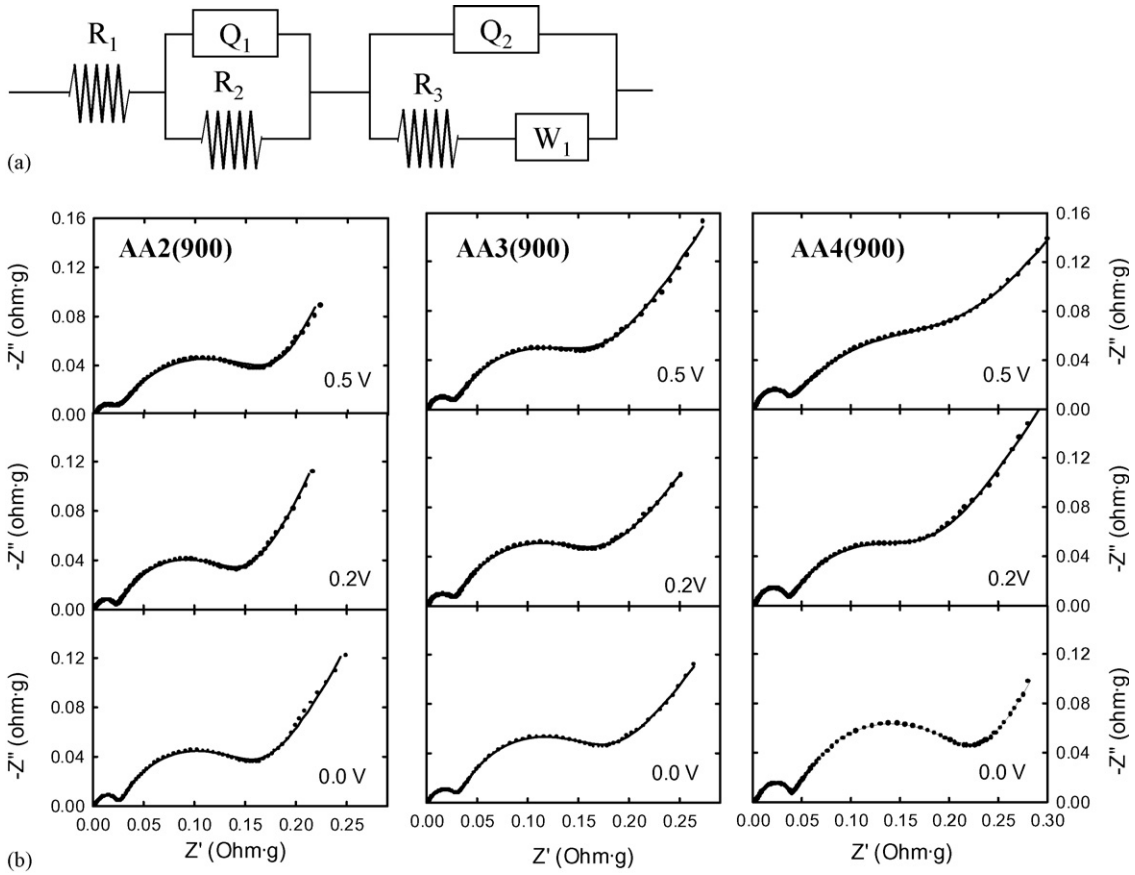

Fig. 6. (a) Analogue circuit for the fitting of the impedance response. (b) Nyquist plots recorded for carbonised samples after the first discharge at several cell potentials. Experimental (dotted line) and fitted curves (solid line) are displayed. For the sake of comparison, resistance values were mass normalised.

reversible insertion in carbon particles, leads to lower capacity values as compared with AA2(900) and AA3(900) samples.

Extended galvanostatic cycling also shows evidence of clear differences in the electrochemical performance (Fig. 5). Thus, AA2(900) and AA3(900) samples show higher capacities and good capacity retention as compared with AA4(900) when cycled at C/50. The differences were more marked when the rate of the reaction was increased to C/10 from C/50. Thus, a large irreversible capacity is observed during the first cycle and the capacity values decrease sharply in subsequent discharges for AA4(900). For the other samples, a significantly lower decrease of capacity is observed after the first cycle and an efficiency value around 85% can be calculated from the second to twentieth cycle. The highest oxygen content in AA4(900) involves an extended irreversible reaction of lithium ions ascribable to lithium trapping at the oxygenated functional groups located on the surface or at void spaces [25,15]. The formation of an extremely thick passivating layer hinders the ionic/electronic connectivity among carbon particles, which affect the kinetics of the electrochemical process. This fact will be further discussed from the impedance plots. Otherwise, the morphology of AA2(900) and AA3(900) samples, characterised by a fluid texture and layered particles, provides a suitable path which could favour the lithium migration among carbon bulk particles. Although the capacity is initially higher for AA3(900), its lower capacity retention at C/50 leads to a fast decrease in capacity. This fact was avoided by increasing the reaction rate to C/10. Likely, the higher content in N and S heteroelements for AA3(900) provides a more reactive surface which irreversibly traps lithium atoms on cycling.

Electrochemical impedance spectroscopy (EIS) allows us to determine the changes in interfacial resistance taking place during the reactions with lithium, which affect the kinetics of the electrochemical reaction. Fig. 6b shows the Nyquist plots for the first discharge. The resistance values have been mass normalised to facilitate comparison. The electrodes were potentiostatically discharged up to the selected voltage and allowed to relax for several hours before the measurement. Two depressed semicircles at high and intermediate frequencies, and a straight line in the low frequency extreme, characterize these curves at low potentials. These experimental data were fitted to the equivalent circuit in Fig. 6a [16,17] from which R_1, R_2 and R_3 values could be calculated. R_1 is the electrolyte solution resistance. R_2 is ascribed to the resistance imposed to lithium migration through the solid electrolyte interface (SEI) irreversibly formed during cell discharging. R_3 is assigned to the resistance occurring during the charge transfer reaction taking place when lithium atoms go values through the interface at the carbon particle surface. The magnitude of R_2 and R_3 is closely related to the corresponding semicircle diameter. The semicircle depression is caused by the presence of inhomogeneities in the electrode material such as roughness, porosity and/or polycrystalline state, which hinder

the frequency dispersion in the interface [30]. Constant phase elements (Q) in parallel with the resistances were used to fit the depressed semicircles. Finally, a Warburg component (W) was introduced to fit the response of the system to the Li^+ diffusion through the intercalated carbon.

Sample AA4(900) shows the highest R_2 value indicating that its specific particle morphology is more prone to develop less conducting surface films. On increasing the lithium content in the carbonaceous electrodes, we detected a slight increase of the surface film resistance (R_2), which is particularly evident for sample AA4(900) by the increasing diameter of the circles at intermediate frequencies in Fig. 6 on decreasing the discharge voltage. This fact seems to evidence that the formation and growth of this layer would not be strictly limited to the 1 V region, but to lower cell potential even in a minor extent. For all samples, the charge transfer resistance (R_3) showed minor changes below 0.5 V with the highest impedance values recorded for the fully discharged AA4(900) sample.

Fully discharged cells were stored at 60 °C for a period of time. Then the EIS were measured with the aim to evaluate the stability upon prolonged storage. Fig. 7a and b show the changes observed in R_2 and R_3. A better stability of the surface film was observed for AA4(900) sample after 7 days, even if the initial values was higher as previously discussed. In contrast, charge-transfer resistance strongly increased for AA2(900) and AA4(900) samples after 7 days.

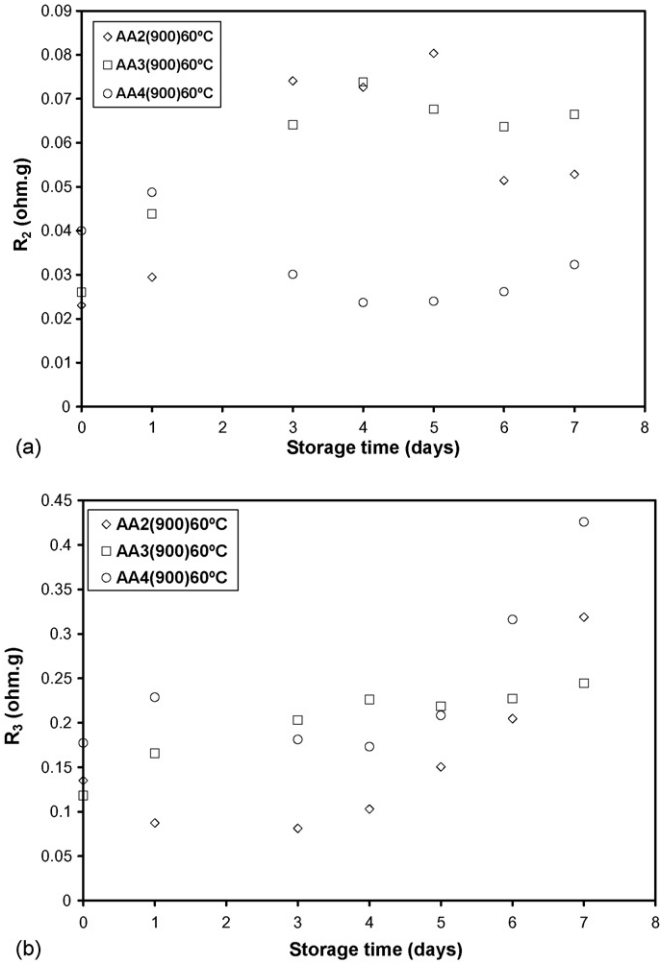

Fig. 7. Variation of SEI and charge transfer resistances vs. storage time at 60 °C for carbonised samples.

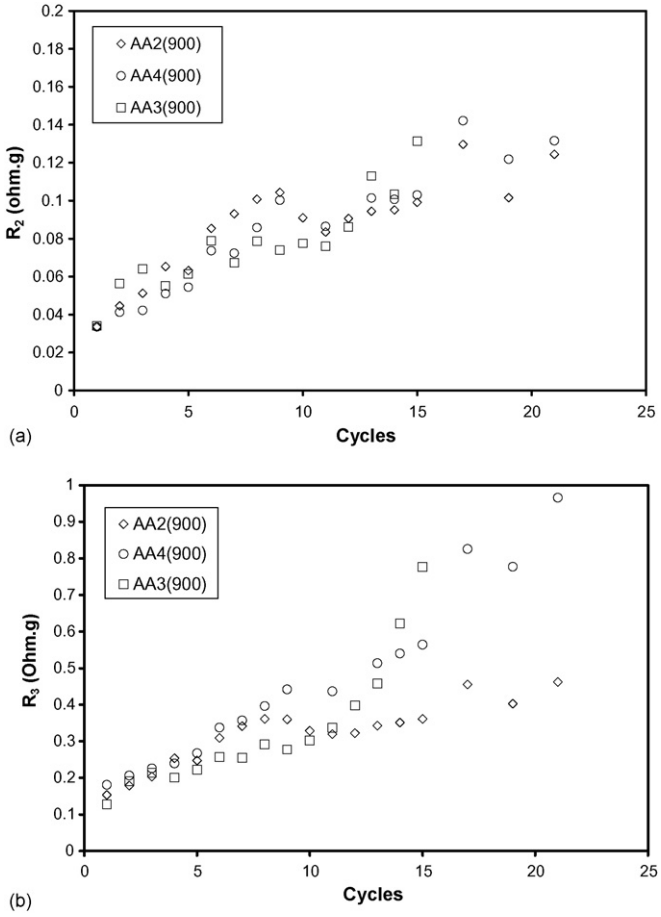

Fig. 8. Variation of SEI and charge transfer resistances vs. cycle number for carbonised samples.

The changes in R_2 and R_3 values were monitored upon cycling (Fig. 8a and b). Although the passivating effect of the SEI has been widely documented [31–33], passivation cannot be considered complete after the first discharge, as the R_2 values continuously increased along the measured range. Similar result has been also found for graphitised samples, which was ascribed to structural instability resulting in graphite microexfoliation from repeated cycling [34]. Thus, the repeated cycling could somehow alter the particle morphology by increasing the surface area exposed to the reaction with the electrolyte. Besides, any clear tendency can be inferred from the comparison among samples. Therefore, the observed differences in the electrochemical behaviour of the samples described above cannot be particularly attributed to different properties of the surface films. R_3 values also show a continuous increase for the first cycles with no marked differences between samples up to the fifth cycle. From this cycle, AA2(900) sample retained lower resistance values for the measured range, while the other samples notoriously increased the R_3 values. This result can explain the better capacity retention of AA2(900) sample upon cycling.

To throw light on the mechanism of the reaction with lithium and to interpret the differences in the electrochemical properties of our carbonaceous materials, ^{7}Li MAS NMR spectra were obtained for the electrodes discharged at 0.2 and 0 V and also for those charged at 2.1 V. Figs. 9–11 show the experimental and calculated spectra, while the corresponding NMR parameters are also included in Table 3. At 0.2 V, all samples have a similar profile, which can be deconvoluted in three different components (Fig. 9 and Table 3). In all cases, a component located at 40–45 ppm ascribable to first-stage LiC_6 in graphitised materials was not observed. This fact is not striking due to the highly disordered structures of carbons obtained below 1000 °C. The shoulder located beneath 1 ppm (peak 1) is usually ascribed to complex products from the electrolyte decomposition yielding the passivating layer. Although the precise nature of the lithium decomposition products cannot be discerned from this unique signal, numerous works have proved the presence of $ROCO_2Li$, Li_2CO_3, ROLi and salt reduction products by vibrational techniques [35–37]. The most intense signal at this potential is

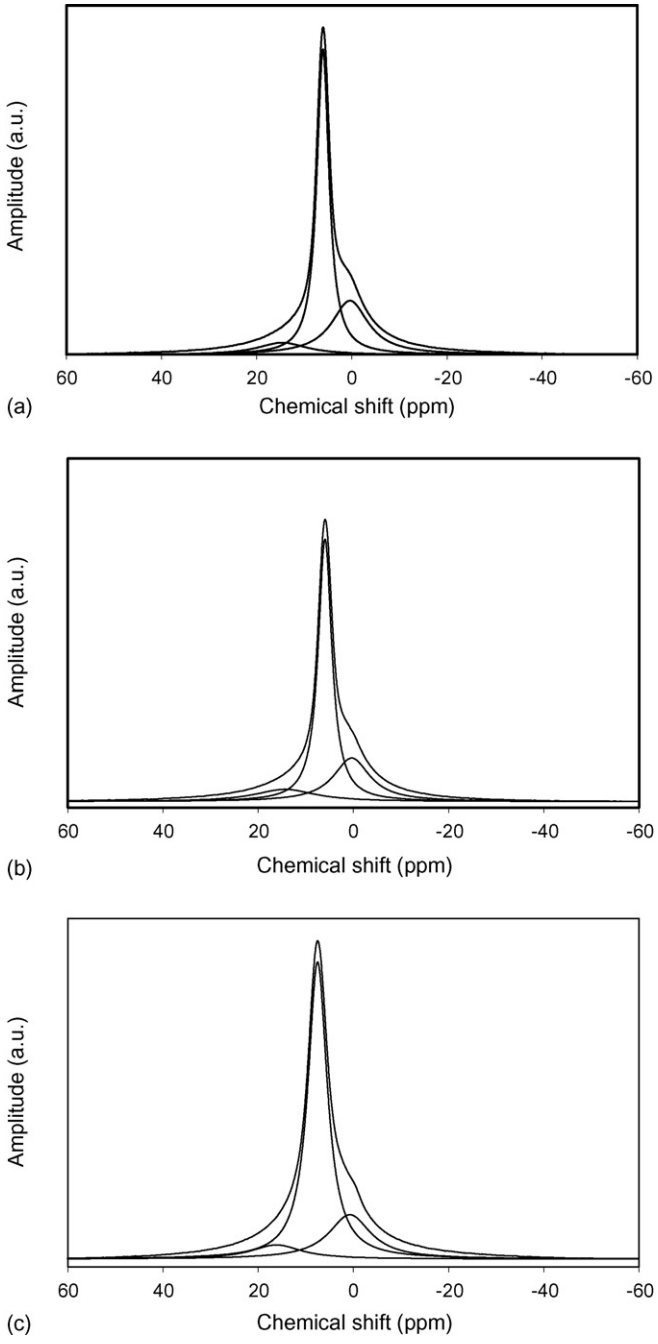

Fig. 9. ^{7}Li NMR spectra of partially discharged electrodes at 0.2 V of the (a) AA2(900), (b) AA3(900) and (c) AA4(900) carbonised samples.

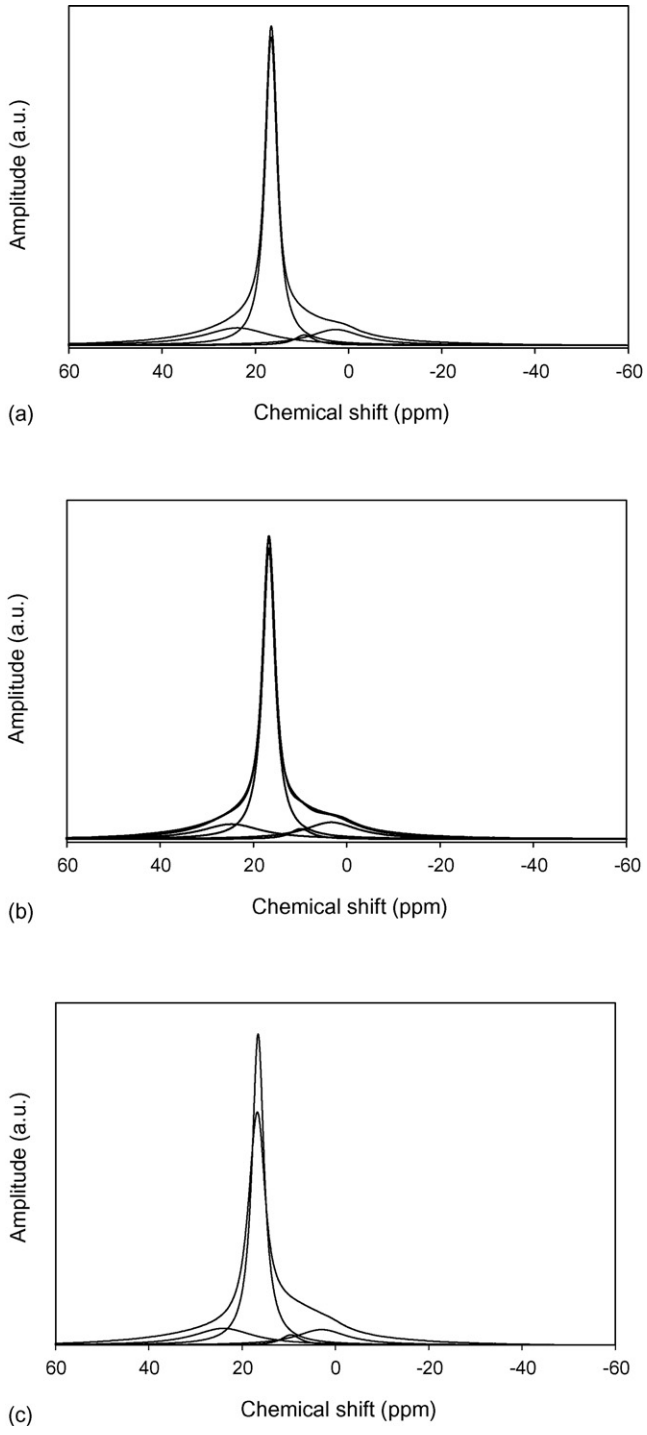

Fig. 10. ^{7}Li NMR spectra of fully discharged electrodes of the (a) AA2(900), (b) AA3(900) and (c) AA4(900) carbonised samples.

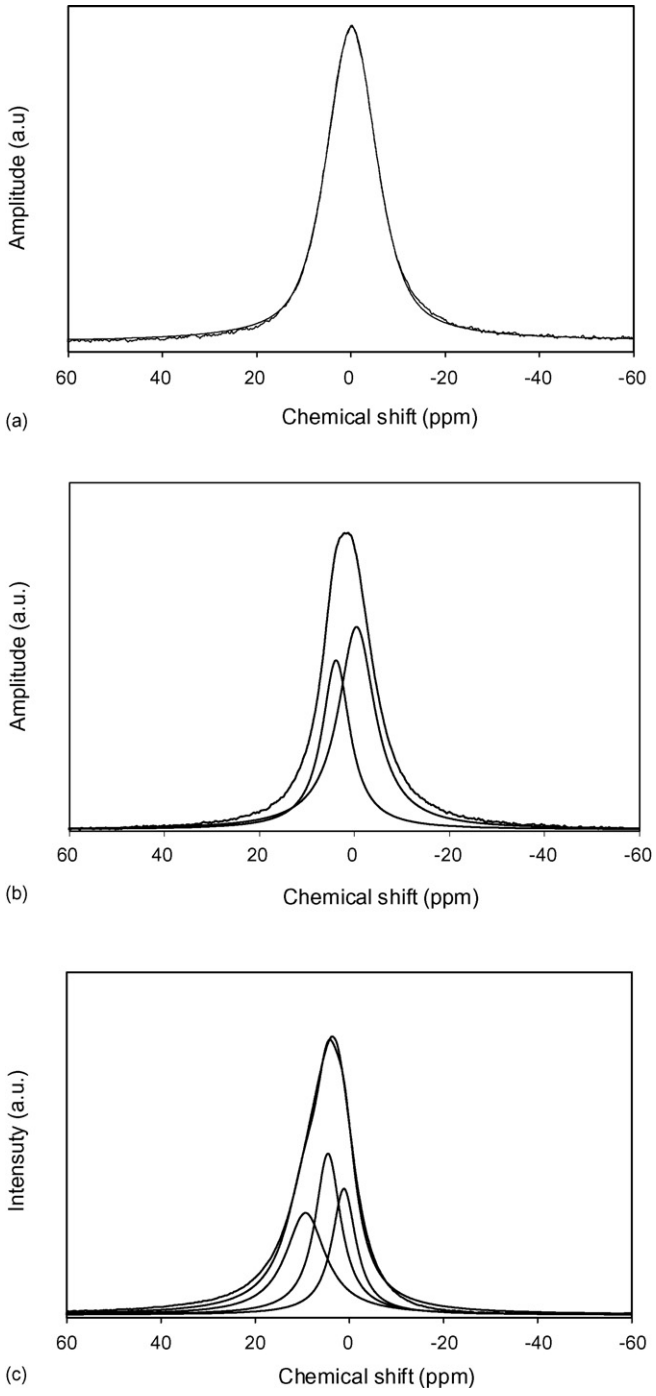

Fig. 11. ^{7}Li NMR spectra of fully charged electrodes at 2.1 V of the (a) AA2(900), (b) AA3(900) and (c) AA4(900) carbonised samples.

located at ca. 6–7 ppm (peak 2). This chemical shift is characteristic of low temperature carbons. Some mechanisms have been proposed to explain the lithium local environment within disorder carbons associated with this low value, including the filling of cavities with lithium clusters [38], or the formation of an ionic complex [39]. However, the former option can be discarded because the formation of clusters with extremely high metal contents must be parallel to the occurrence of Knight shifts due to conductive electrons. In our spectra such signal could not be detected. Thus, this peak must be assigned to ionic

Table 3
Parameters of ^{7}Li MAS NMR spectra

Parameter	V	CS (ppm)	Width (ppm)	C (%)
AA2	0.2	0.37	9.35	31.3
		6.05	3.13	59.09
		14.60	12.74	9.61
AA3	0.2	0.34	9.25	26.74
		5.95	3.46	61.24
		14.37	15.40	12.02
AA4	0.2	0.74	10.66	22.4
		7.51	4.91	69.03
		16.16	12.79	8.58
AA2	0	2.75	13.53	14.00
		9.47	5.18	3.49
		16.57	3.11	62.69
		23.82	17.39	19.82
AA3	0	3.30	13.87	15.93
		9.83	5.41	3.86
		16.66	3.23	64.23
		24.67	15.54	15.98
AA4	0	2.94	13.24	13.89
		9.54	5.07	3.51
		16.57	3.12	65.01
		23.99	15.54	17.58
AA2	2.1	0.15	12.59	100.00
AA3	2.1	−0.47	9.40	61.35
		3.86	7.09	38.65
AA4	2.1	1.14	6.20	26.92
		4.53	6.65	36.92
		9.30	10.31	36.16

lithium stored in the neighbourhood of highly pinned graphene areas in which lithium ions have low mobility or linked to aromatic rings constituting organometallic complex such as lithium naftalene [40]. A third weak signal is simultaneously observed at 14–16 ppm (peak 3). This signal is also commonly reported for low temperature carbons. Its low value does not allow to be strictly ascribed to insertion in large graphene layers rather than to less covalently bonded Li [41]. By comparing the peak contributions of the samples discharged at 0.2 V, a decrease in the peak 1 from AA2(900) to AA4(900) samples can be associated with the loss of particle roughness detected by SEM for AA4(900). It would lead to a small surface area in which the SEI film could be grown. Conversely, the absolute contribution of peak 2 increased from AA2(900) to AA4(900) what can be attributed to the high oxygen and hydrogen content in the latter sample. These heteroatoms are the responsible of highly pinned graphene domains in which lithium can be either restrained in mobility or irreversibly linked to the heteroatoms.

The complete discharge of the lithium cell yielded carbon electrodes with ^{7}Li NMR spectra characterised by a new component at a lower field (peak 4) (Fig. 10 and Table 3). This new signal is centered at ca. 24 ppm and is a major component of the spectrum. Resonances with similar shifts have been previously reported for carbons prepared over 2000 °C and related to lithium insertion between graphene layers with conducting electrons responsible for the Knight shift but stacked in a less ordered sequence than graphite layer [42] or in less extended domains. In our spectra, this new component contributed with

only a small percentage as expected from the low temperature of carbonisation. From the observation of the discharge electrodes deconvoluted spectra, we can discern that the evolution of the peaks do not correspond to a shifting of a unique signal over the whole range of chemical shifts. Rather, the progressive lithium reaction during discharge seems to involve the successive appearance and intensity changes of the component signals described above. Parallel to the increase in intensity, the peaks are shifted to low fields in a limited interval of ppm as lithium content is increased (Table 3). In any case, the first full discharge does not involve significant differences in the spectra among samples.

On charging to 2.1 V (Fig. 11 and Table 3), important differences are observed. The peaks at low field tend to disappear while peaks near 0 ppm regain their intensity. AA2(900) sample leads to a ^{7}Li NMR single component profile centered near 0 ppm that indicates that inserted lithium ions are reversibly extracted from carbon material, while the signal at 0 ppm corresponds to those lithium compounds (e.g. lithium carbonates and alkyl carbonates) irreversibly produced during the formation of the SEI. On increasing the treatment time, low field components are more clearly evidenced. In fact, peaks 2 and 3 are the most intense signals for AA4(900) sample. This result would confirm the lower reversibility of lithium reaction and allow us to assign it to the partially reversible linking established between lithium and heteroatom-rich carbon zones.

4. Conclusion

The oxidative stabilisation treatment has been applied to cokes obtained from anthracene oils. The influence of the extension used for the air treatment has been evaluated to elucidate the limit from which the advantages of structural retention are counterbalanced by an excessive surface absorption of oxygen. High contents of this element yield functional groups that irreversibly trap lithium ions at the carbon surface. The chemical composition data show marked differences for the sample treated for 12 h as compared to samples oxidised for shorter periods. A high content of oxygen was detected that contributes to increase the softening points. As a consequence, SEM micrographs for AA4(900) sample exhibits less layered particles. It is likely that the elevated presence of oxygen atoms at the edge of the particles hindered the condensation of graphene particles and the graphitisation process is actually impeded.

The differences in the physicochemical properties are reflected in the poorer electrochemical behaviour observed for this sample. Thus, a higher irreversibility during the first discharge, lower reversible capacities in successive cycles and higher resistance values for the charge transfer reaction were measured. In fact, ^{7}Li MAS NMR spectra recorded on samples during the first cycle evidenced different lithium local environments whose contributions evolved according to the cell potential from lithium in less organised regions to intercalated ions affected by the conducting electrons in graphene layers, which prevail near 0 V. Relevant differences among samples are observed at the end of the first charge. Sample AA2 is characterised by residual Li^{+} located at the SEI film, while AA4 showed the presence of Li in less organised regions and irreversibly trapped in highly pinned graphene layers or links with heteroatoms. The observed differences give a direct explanation of the different electrochemical behaviour of these samples as compared to those samples prepared at short annealing times. Summarising, the beneficial use of oxidative stabilisation derived from the retention of the anisotropy in the carbon structure is certainly limited by the use of extended treatments.

Acknowledgments

The authors are grateful to CICYT for financial support (Contract MAT2002-00434 and contract MAT2001-1694), NMR service of the University of Córdoba and M.C. Mohedano for her technical support. R.A. is indebted to MCYT (programa Ramón y Cajal). A. Concheso is indebted to MCYT for his predoctoral grant.

References

[1] K. Sawai, T. Ozhuku, T. Hirai, Chem. Exp. 5 (1990) 837.
[2] T. Ozhuku, Y. Iwakoshi, K. Sawai, J. Electrochem. Soc. 149 (1993) 2490.
[3] V. Manev, I. Naidenov, B. Puresheva, P. Zlatilova, G. Pistoia, J. Power Sources 55 (1995) 211.
[4] B. Simon, S. Flandrois, K. Guerin, A. Fevrier-Bouvier, I. Teulat, P. Biensan, J. Power Sources 81-82 (1999) 312.
[5] A.N. Dey, B.P. Sullivan, J. Electrochem. Soc. 117 (1990) 222.
[6] R. Alcántara, M. Jaraba, P. Lavela, J.L. Tirado, J. Electrochem. Soc. 151 (2004) A53.
[7] R. Alcántara, M. Jaraba, P. Lavela, J.M. Lloris, C. Perez Vicente, J.L. Tirado, J. Electrochem. Soc. 152 (2005) A13–A18.
[8] L. Aldon, A. Garcia, J. Olivier-Fourcade, J.C. Jumas, F.J. Fernández-Madrigal, P. Lavela, C. Pérez-Vicente, J.L. Tirado, J. Power Sources 119–121 (2003) 585–590.
[9] L. Aldon, P. Kubiak, M. Womes, J.C. Jumas, J. Olivier-Fourcade, J.L. Tirado, J.I. Corredor, C. Pérez-Vicente, Chem. Mater. 16 (2004) 5721.
[10] R. Alcántara, M. Jaraba, P. Lavela, J.L. Tirado, J.C. Jumas, J. Olivier-Fourcade, Electrochem. Comm. 5 (2003) 16.
[11] R. Alcántara, P. Lavela, G.F. Ortiz, J.L. Tirado, R. Stoyanova, E. Zhecheva, J.M. Jiménez-Mateos, J. Electrochem. Soc. 151 (2004) A2113.
[12] J.R. Dahn, T. Zheng, Y. Liu, J.S. Xue, Science 270 (1995) 590.
[13] Y.-C. Chang, H.-J. Sohn, Y. Korai, I. Mochida, Carbon 36 (1998) 1653.
[14] D.A. Stevens, J.R. Dahn, J. Electrochem. Soc. 148 (2001) A803.
[15] C.W. Park, S.-H. Yoon, S.I. Lee, S.M. Oh, Carbon 38 (2000) 995.
[16] A. Concheso, R. Santamaría, M. Granda, R. Menéndez, J.M. Jiménez-Mateos, R. Alcántara, P. Lavela, J.L. Tirado, Electrochim. Acta. 50 (2005) 1225.
[17] A. Concheso, R. Santamaría, R. Menéndez, J.M. Jiménez-Mateos, R. Alcántara, P. Lavela, J.L. Tirado, J. Solid State Electrochem. 9 (2005) 627.
[18] M. Pérez, M. Granda, R. García, R. Santamaría, E. Romero, R. Menéndez, J. Anal. Appl. Pyrolysis 63 (2002) 223.
[19] M.D. Guillén, M.J. Iglesias, D. Domínguez, C.G. Blanco, Energy Fuels 6 (1992) 518.
[20] P. Scherrer, Math. Phys. 2 (1918) 98.
[21] B.E. Warren, X-Ray Diffraction. Addison-Wesley, Reading, Massachusetts. 0 (1969) 251.
[22] D. Massiot, F. Fayon, M. Capron, I. King, S. Le Calvé, B. Alonso, J.O. Durand, B. Bujoli, Z. Gan, G. Hoatson, Magn. Reson. Chem. 40 (2002) 70.
[23] Y.P. Wu, C. Jiang, C. Wan, R. Holze, Electrochim. Acta. 48 (2003) 867.
[24] Y.P. Wu, C. Jiang, C. Wan, R. Holze, Solid State Ionics 156 (2003) 283.
[25] D. Larcher, C. Mudalige, M. Gharghouri, J.R. Dahn, Electrochim. Acta 44 (1999) 4069.
[26] M. Inaba, H. Yoshida, Z. Ogumi, J. Electrochem. Soc. 143 (1996) 2572.

[27] C. Blanco, R. Santamaría, J. Bermejo, R. Menéndez, Carbon 35 (1997) 1191.
[28] J.-S. Kim, J. Power Sources 97–98 (2001) 70.
[29] M. Monthioux, M. Oberlin, A. Oberlin, X. Bourrat, R. Boulet, Carbon 20 (1982) 167.
[30] J.R. Macdonald, Impedance Spectroscopy, Emphasizing Solid Materials and Systems, Wiley, USA, 1987.
[31] A.N. Dey, B.P. Sullivan, J. Electrochem. Soc. 117 (1970) 222.
[32] D. Aurbach, Y. Eli-Eli, J. Electrochem. Soc. 142 (1995) 99c.
[33] R. Fong, U. von Sacken, J.R. Dahn, J. Electrochem. Soc. 137 (1990) 2009.
[34] D. Aurbach, B. Markovsky, M.D. Levi, E. Levi, A. Schechter, M. Moshkovich, Y. Cohen, J. Power Sources 81-82 (1999) 95.
[35] D. Aurbach, B. Markovsky, I. Weissman, E. Levi, Y. Ein-Eli, Electrochim. Acta 45 (1999) 67.
[36] D. Aurbach, J.S. Gnanaraj, M.D. Levi, E.A. Levi, J.E. Fischer, A. Claye, J. Power Sources 97-98 (2001) 92.
[37] Y. Ein-Eli, B. Markovsky, D. Aurbach, Y. Carmeli, H. Yamin, S. Luski, Electrochim. Acta 3 (1994) 2559.
[38] K. Tokumitsu, A. Mabuchi, H. Fujimoto, T. Kasuh, J. Electrochem. Soc. 143 (1996) 2235.
[39] K. Sato, M. Noguchi, A. Demachi, N. Oki, M. Endo, Science 264 (1994) 556.
[40] N. Takami, A. Satoh, T. Ohsaki, M. Kanda, Electrochim. Acta 42 (16) (1997) 2537.
[41] Y. Daif, Y. Wang, V. Eshkenazi, E. Peled, S.G. Greenbaum, J. Electrochem. Soc. 145 (1998) 1179.
[42] K. Tatsumi, T. Akai, T. Inamura, K. Zhagib, N. Iwashita, S. Higuchi, Y. Sawada, J. Electrochem. Soc. 143 (1996) 1923.